

Spin-lattice Coupling and Magneto-dielectricity in $\text{Ca}_3\text{Mn}_2\text{O}_7$ Layered Perovskite

*Pooja Sahlot, Gaurav Sharma, Vasant Sathe, and Anand Mohan Awasthi**

UGC-DAE Consortium for Scientific Research, University Campus, Khandwa Road, Indore-452 001, India.

*E-mail: amawasthi@csr.res.in

Keywords: layered perovskite, spin-lattice coupling, magneto-dielectricity, relaxor-like dipolar-correlations, non-linear permittivity

Abstract: Dielectric study on $\text{Ca}_3\text{Mn}_2\text{O}_7$ features relaxor-like segmented dynamics below the antiferromagnetic ordering. Dipolar relaxations of different origin are spectrally resolved exhibiting distinct H -field alterations. This identifies their allegiance to different magnetic sub-phases and establishes dual coupling of electrical, magnetic, and structural degrees of freedom. Further, strong spin-lattice coupling has been affirmed with Raman spectroscopy across the magnetic ordering. Short-range electrical correlations collaterally cause measurable harmonic dielectric response in the system. The χ_3^e -susceptibility signal yields genuine harmonic magneto-dielectricity, consistent with but exhibiting two orders of magnitude larger H -field effect, vis-à-vis that obtained in the fundamental dielectric constant ϵ' .

Introduction

Interesting evolution of magnetic and electrical configurations has been realized in layered Ruddlesden-Popper (R-P) compounds, with inter-coupled structural, magnetic, and electric properties. R-P series compounds are represented as $\text{A}_{n+1}\text{B}_n\text{O}_{3n+1}$ for 2+ valence state ‘A’ cations and 4+ valence ‘B’ ions, with C usually being oxygen (2- valence).^[1] Structurally, they reveal themselves as integral- n ABO_3 perovskite blocks, with inserted AO sheets in-between, along the c -axis. Here layered structure has open doors to many interesting properties. $\text{La}_{1.4}\text{Sr}_{1.6}\text{Mn}_2\text{O}_7$ has been shown to possess inter-planar tunneling induced low-field magneto-resistance.^[2] Development of ferromagnetic clustering in the long range antiferromagnetic (AFM) ordering has been reported in $n=3$ R-P compound $\text{La}_{3-x}\text{Sr}_{1+3x}\text{Mn}_3\text{O}_{10}$.^[3] Further, in R-P compounds the ferroelectric mechanism has been described

via combination of two octahedral distortion patterns namely “hybrid improper ferroelectricity”.^[4] Hybrid improper ferroelectricity (HIF) supported by first-principles calculation has been evident in $n=2$ R-P compound; $\text{Ca}_3(\text{Ti,Mn})_2\text{O}_7$.^[5,6] Thus compared to simple-perovskites these distortions offer scope for magneto-electric (ME) coupling and multiferroicity in these layered structures; since unfulfilled d -orbital accommodated in the oxygen octahedra favors (anti)ferromagnetism, which relates profoundly with the metal-oxygen-metal bond angles.^[7]

$\text{Ca}_3\text{Mn}_2\text{O}_7$ R-P system exhibits structural transition from $I4/mmm$ tetragonal phase to inversion-symmetry-breaking $\text{Cmc}21$ orthorhombic phase, with introduction of octahedral rotation in (001) plane, along with the octahedral tilt about [100] axis.^[8] The structural transition covers a wide (300-600K) temperature range, with coexistent tetragonal and orthorhombic phases.^[9] In pure orthorhombic phase, relaxor behaviour has been suggested below the room temperature.^[9] Because of the high leakage-current at high temperatures in the orthorhombic phase, there have been difficulties in experimentally ascertaining ferroelectricity in the system.^[7] Upon cooling, dielectric losses get reduced and ferroelectricity with measurable polarization is detected below 60K, which can be further explored at lower temperatures.^[9] Here, emphasis on $n=2$ R-P manganite $\text{Ca}_3\text{Mn}_2\text{O}_7$ is due its expected candidacy for ME coupling.^[4] Complementarily to ferroelectricity, octahedral tilting supports weak ferromagnetism and octahedral rotation induces magneto-electricity in this system.^[10] Electric field tunability of these octahedral rotations is expected to enhance the ME effect. From first-principles calculations, Benedek and Fennie have reported G-type antiferromagnetic (AFM) ground state for the system, with a net perpendicular spin-canted moment via spin-orbit (S-O) interactions.^[4] Dzyaloshinskii’s criteria explain the canted moment via the oxygen-octahedral tilt distortion. In $\text{Ca}_3\text{Mn}_2\text{O}_7$ system, antiferromagnetic transition with Néel temperature 123K, along with the emergence of weak ferromagnetism (WFM) below 110K, have been reported previously.^[11] Dzyaloshinskii-Moriya (D-M)

interaction favored WFM clusters' formation in the AFM-matrix, inducing an exchange-bias (EB), was characterized in detail.^[11,12] Here, we present the linear/non-linear dielectric properties of $\text{Ca}_3\text{Mn}_2\text{O}_7$, and their correlation with magnetic-evolution/phase-mixing is compared & distinguished. Here non-linear dielectric measurements compliment the understanding of electrical structure from linear measurements, giving more profound effect of change in magnetic-configuration on dipolar-correlations compared to latter. Magneto-dielectricity (linear and non-linear) is explored under applied magnetic field, across a sufficiently wide temperature range covering the AFM ordering at $T_N = 123\text{K}$.

Experimental Details

Single phase polycrystalline $\text{Ca}_3\text{Mn}_2\text{O}_7$ was synthesized at 1300°C by conventional solid state synthesis technique. Structural characterization by powder XRD using Bruker D8 advance diffractometer with Cu-K_α X-ray radiation ($\lambda = 1.5405 \text{ \AA}$) confirms orthorhombic structure with lattice parameters obtained as, $a = 19.40(8) \text{ \AA}$, $b = 5.24(3) \text{ \AA}$, and $c = 5.25(2) \text{ \AA}$, as reported previously.^[11] Raman scattering measurements on $\text{Ca}_3\text{Mn}_2\text{O}_7$ system have been performed with HR800 Jobin-Yvon spectrometer, in the temperature range of 5K to 300K, using He-Ne laser of wavelength 632.8 nm. Low temperature fundamental dielectric response and magneto-dielectricity along with second harmonic measurements have been performed in parallel-plate capacitor configuration, from 200K down to 7.5K in the frequency range of 50 Hz to 300 kHz, using NovoControl Alpha-A Broadband Impedance Analyzer and Oxford NanoSystems Integra 9T magnet-cryostat.

Results

Raman Spectroscopy: To explore the spin-lattice coupling in the system via study of vibrational modes, Raman scattering measurements have been performed. Predicted Raman active optical modes for the system with $\text{Cmc}21$ space group are $18A_1 + 17A_2 + 16B_1 + 18B_2$. The Raman spectrum depicting phonon modes for the sample are shown in **figure 1(a)**, in the temperature range of 5K to 300K. The two most prominent phonon modes have been

recognized as $A_1^{(15)}$ and $A_1^{(17)}$ for the Cmc21 phase (=A21ma structure with ‘ c ’-long axis).^[13] Lorentzian peak-fit analysis (**figure 1(b) and 1(c)**) has been carried out for the respective modes, to obtain thermal evolution of the phonon modes. Peak-characteristics follow the classical behaviour; frequency-shifts decrease and line-widths broaden with increase in temperature. This is accompanied by sharp changes in the frequency-shifts at ~ 105 K; shown in **figure 1(d)** (left-pane) for $A_1^{(15)}$ mode and in **figure 1(e)** (left-pane) for $A_1^{(17)}$ mode, which independently confirm the spin-lattice coupling in the system. Line-widths of the respective modes have also been studied, which relates to the decay/lifetime of the phonons involved. Concurrent kinks in the line-widths again at ~ 105 K, shown in figure 1(d) (right-pane) and figure 1(e) (rightpane) for $A_1^{(15)}$ and $A_1^{(17)}$ modes respectively, establish the spin-lattice coupling.

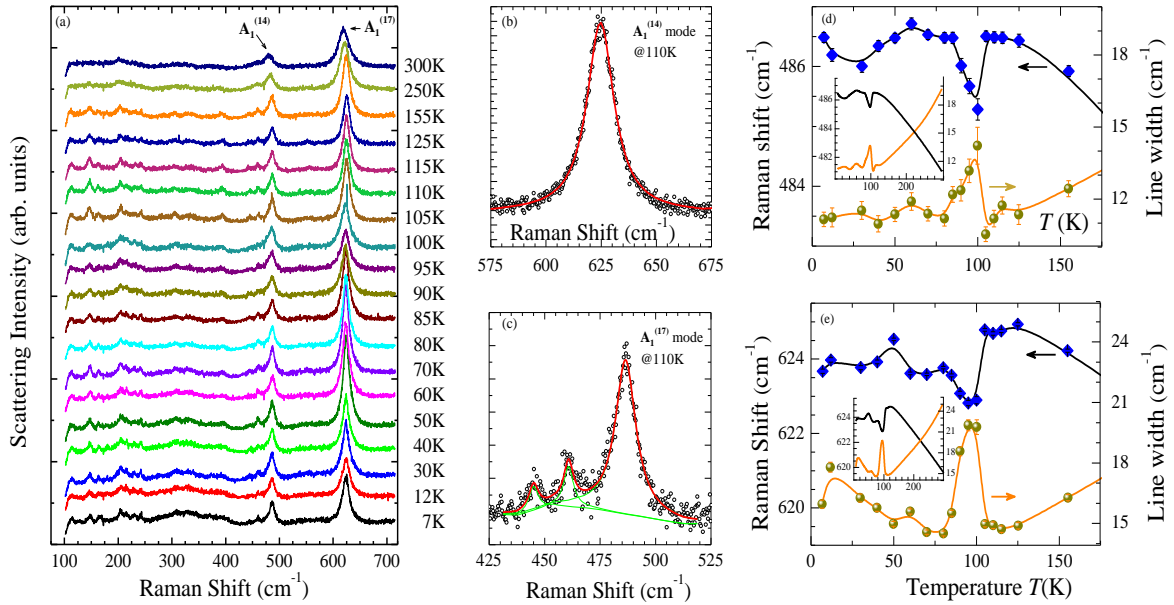


Figure 1. (a) Obtained Raman spectra from room temperature down to 7K. (b), (c) Lorentzian peak-fit for $A_1^{(15)}$ mode and $A_1^{(17)}$ mode respectively. (d) Temperature dependence of Raman shift (left-pane) and line-width (right-pane) obtained for $A_1^{(15)}$ mode. (e): Temperature dependence of Raman shift (left-pane) and line-width (right-pane) obtained for $A_1^{(17)}$ mode.

Signals corresponding to the co-existing WFM-phase (below 110K) in the AFM-matrix phase ($T_N=123\text{K}$) are thus clearly revealed in the Raman study. Here, $A_1^{(15)}$ phonon mode mainly involves atomic motion of O1(-z), O3(z), and O4(z), along the z-axis (being the a -axis here) with in phase motion of O3 and O4. $A_1^{(17)}$ phonon mode characterizes in phase motion of O3(z), O4(z) atoms and stretching type motion of O1(z) atom. The change in the phonon modes across WFM further establishes the effective contribution from O1-atomic motion along the a -axis, in concurrence with the decrease in Mn-O1-Mn bond angle, obtained in the SXRD data analysis.^[10] This explains that the Mn-O₆ octahedra-distortion related changes in the Mn-O-Mn bond angles induce changes in the magnetic configuration. Here, Raman study establishes that the WFM is associated with the inter-octahedral changes connected via O1-atom along the a -axis. This suggests low dimensionality of the WFM phase in this system.

Dielectric Spectroscopy: Figure 2(a) presents the dielectric constant $\epsilon'_f(T)$ of $\text{Ca}_3\text{Mn}_2\text{O}_7$ at various frequencies. Here, sharp frequency-dependent step-change in $\epsilon'_f(T)$ is observed. At high- T 's, relaxation times $\tau(T)$ are small enough that even at higher radio frequencies (RF) condition $2\pi f\tau(T) < 1$ applies; resulting in a rather small frequency-dependence of $\epsilon'_f(T)$, as observed. Cooling in the orthorhombic phase develops polar correlations; manifest here as step-like (thermally-activated) decrease of the dielectric constant. Thus-increased $\tau(T)$ leads to resonance of the measurement frequency and the response timescale of the correlated dipoles ($2\pi f\tau(T) = 1$); which marks maximum slopes (inflexion-points) of $\epsilon'_f(T)$, at successively lower frequencies upon cooling. Here, the correlations produce size-dispersed dipole-clusters, each responding optimally at different frequency ($\omega_p(T) \sim 1/\text{cluster-size}$), which shows up in thermally activated dielectric spectra. For a given measurement frequency, super-resonance ($2\pi f\tau(T) > 1$) condition upon further cooling causes the roll-off of $\epsilon'_f(T)$ to lower values, for the same inertial reason as occurs for the $\epsilon'_f(f)$ -isotherms at high frequencies.

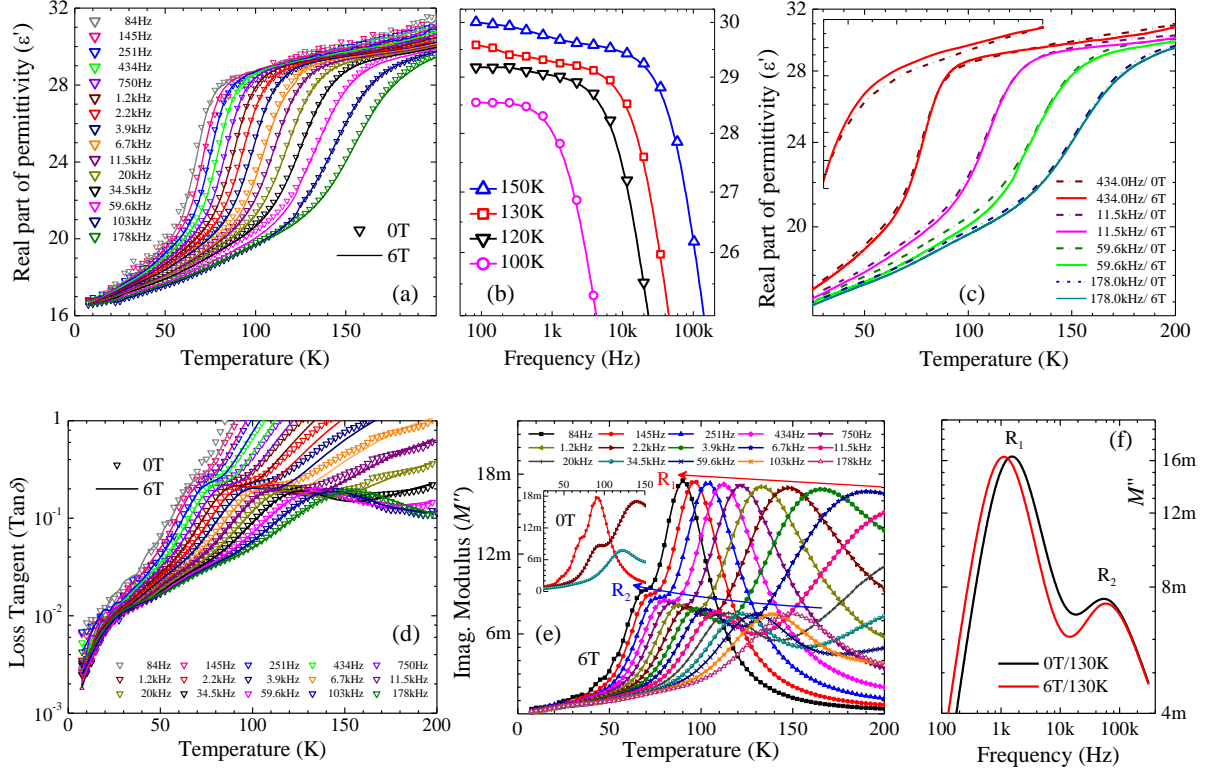


Figure 2. (a) Temperature dependent dielectric constant at different frequencies. (b) frequency dependence of dielectric constant at temperatures: 100K, 120K, 130K & 150K. (c): $\epsilon'(T)$ at selected frequencies under zero- and 6T magnetic field. (d): Temperature dependent loss-tangent at different frequencies, under zero- and 6T magnetic field. (e): Modulus $M''(T)$ isochrones under 6T applied H -field at various frequencies. Inset shows representative isochrones without the H -field. (f): frequency dependence of Modulus $M''(f)$ at 130K under 0T- and 6T-field.

In layered perovskites, FE-instability consists of O6-octahedron rotations, with negligible off-centering of the B-site cation. The associated energy-gain (due to lattice-strain) and energy-loss (due to dipole-dipole interaction) here rather settle in introducing antiferro-distortive (AFD) -like features over a temperature window, thereby suppressing the long-range FE-ordering in the system at a sharp transition temperature.^[14,15] In the quantum paraelectric-like AFD systems, chemical substitution, application of electric field, or dimensional-strain can

induce the FE.^[16] In the layered $\text{Ca}_3\text{Mn}_2\text{O}_7$, no specific heat anomaly pertaining to a long-range FE transition is observed below the room temperature.^[17]

Change in $\varepsilon'(T)$ produced under H -field is zoomed-on in **figure 2(c)**, at selected frequencies.

At temperatures above the $\varepsilon'_f(T)$ -step, H -field enhances correlations between the dipoles, evident from $\varepsilon'(6\text{T}) < \varepsilon'(0\text{T})$ (figure 2(c)). Also, for frequencies $f \geq 11.5$ kHz, at all temperatures $\varepsilon'_f(T)$ simply reduces under the field. At lower frequencies however, H -field alters the dielectric constant in both +ve and -ve sense over different temperature ranges, depending upon the extent of the dipolar interactions. At probing frequencies $f < 11.5\text{kHz}$, H -field mobilizes the larger/frozen dipolar clusters ($2\pi f\tau_{cl} > 1$; $\varepsilon'(6\text{T}) > \varepsilon'(0\text{T})$ over 80-130K) and consolidates/freezes the smaller ones ($2\pi f\tau_{cl} < 1$; $\varepsilon'(6\text{T}) < \varepsilon'(0\text{T})$ below 80K).

Associated with the step-like change in $\varepsilon'(T)$, relaxation peaks in loss tangent ($\tan\delta = \varepsilon''/\varepsilon'$) are observed, as shown in **figure 2(d)**. Increase in the peak temperature of $\tan\delta_f(T)$ isochrones with rise in frequency depicts thermally activated character. Here we emphasize low values of permittivity with seemingly frequency independent at low frequencies on cooling below 130K (**figure 2(b)**) makes the dielectricity observed for the system to be inter-grain response.

Further $\tan\delta < 1$ for the relaxations excludes contributions from charge carriers for frequencies $\geq 100\text{Hz}$.

For further insight, dielectric modulus (M^*) is observed, which reveals two sets of localized dipole-relaxations in the system.^[18]

$$M^* = 1 \div \varepsilon^* = M' + iM'' \quad (1)$$

$M''(T)$ isochrones shown in **figure 2(e)** reveal two relaxation processes in the system. **Figure 2(f)** depicts $M''(f)$ isotherm at 130K, here relaxation- R_1 well-developed at lower frequencies with higher modulus— persisting to higher frequencies with increase in temperature— and another relaxation- R_2 with comparatively low modulus well-formed at relatively higher frequencies. R_1 -relaxation peaks shifts to lower frequency side with application of H -field

while R_2 -relaxation peak shifts to higher frequency side with H -field application. Our Havriliak-Negami analysis reveals, the corresponding peaks are not Lorentzian (broadening parameters $\alpha, \beta < 1$).^[10]

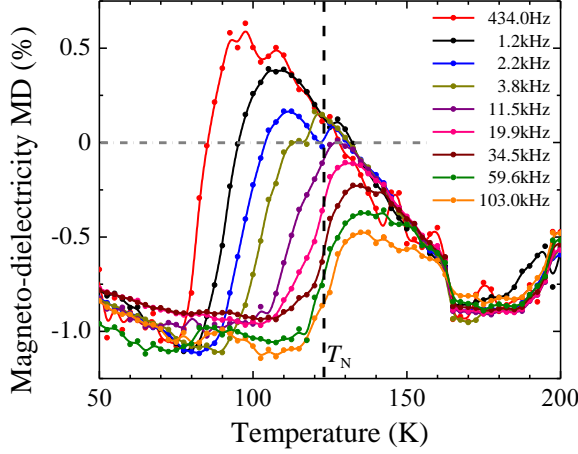


Figure 3. Temperature dependence of Magneto-dielectricity MD(%).

To further correlate electric and magnetic properties of the system, magneto-dielectricity (MD) that is change in dielectric properties under 6 Tesla field has been studied.

$$MD(\%) = \{\varepsilon'(H) \div \varepsilon'(0) - 1\} \times 100 \quad (2)$$

Figure 3 demonstrates temperature dependence of MD(%), depicting all negative MD at temperatures above 130K, while at lower temperatures, both negative and positive MD can be seen (for low frequencies). This is already evident in the zero- and 6T-field $\varepsilon'(T)$ -plots (figure 2(c)) at selected frequencies. In the system low dimensional magnetic ordering are observed even above 123K, which accounts for MD above T_N . Over 80-130K temperature-window, magnetic field suppresses dipole-interactions in larger clusters (c.f., thermal activation), thereby reducing (increasing) the local polarization (polarizability ε'), whereas outside this window, H -field consolidates the growth of smaller-sized dipolar clusters (c.f., thermal de-activation), thereby enhancing (reducing) the local polarization (ε'). The dual nature of MD shows up over the temperature region where consolidating dipolar clusters evolve. The

exclusive orientational-liquid at high- T 's however features only negative MD (i.e., field-enhanced dynamical correlations), as indeed expected.

R_2 - and R_1 -relaxations can be characterized as correlated dipoles which consolidate in wake of the emergent/coupled WFM-nanophase and bulk/AFM-matrix. The application of magnetic field tends to merge the AFM transition with occurrence of WFM favoring the emergence of isolated WFM nano-phase (coexistent with the AFM-matrix) versus phase-separated or uniformly spin-canted configurations. With application of 7T magnetic field the AFM-WFM transition merges and shifts down to 109K.^[10] Since the WFM is accompanied with octahedron distortion in the system, magneto-dielectricity in the system carries this feature showing both correlation and de-correlation of dipolar entities under the H -field, accounting for the positive MD at low-frequencies along with negative MD, over certain temperature window.

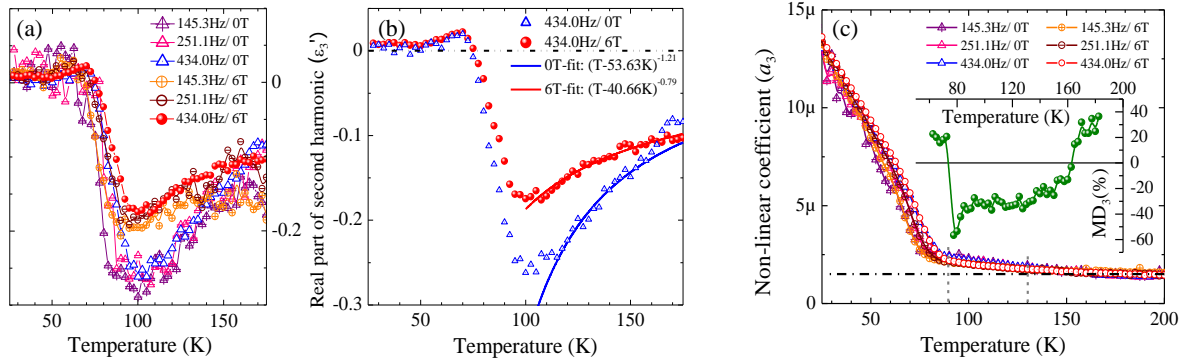


Figure 4. (a): Temperature dependence of second harmonic signal (ϵ'_3) under zero- and 6T-magnetic field. (b): Temperature dependence of ϵ'_3 -signal at 434 Hz with divergence-fit under zero- and 6T-magnetic field. (c): Temperature dependence of a_3 signal under zero- and 6T-magnetic field. Inset: Harmonic magneto-dielectricity $MD_3(\%)$ from the second-harmonic signal.

The magneto-electric effect coupled through structural distortions collaterally manifests in the second-harmonic (ϵ'_3) measurements. Negative-definite $\epsilon'_3(T)$ -signal has been observed,

undergoing through an extremum at $\sim 100\text{K}$, and vanishing near $\sim 50\text{K}$, as shown in **figure 4(a)**. This is in agreement with theoretical modeling for relaxor, exhibiting frequency-dispersive relaxation.^[19,20] The low strength of ε'_3 -signal indicates its major contribution from the term $\sim -\chi_1^4$, denoting cluster-induced relaxor, and not from the bulk polarization term $\sim P^2\chi_1^5$.^[20,21]

Increase of the harmonic signal is expected to diverge critically, with temperature dependence^[22,23]

$$|\varepsilon'_3| \propto (T - T_g)^{-\gamma} \quad (3)$$

From the fits of $\varepsilon'_3(T, H)$ -signals over 115-160K with equation (3) (solid curves in **figure 4(b)**), we obtain $T_g(0\text{T}) = 53.63\text{K}$ as the freezing temperature with divergence exponent $\gamma(0\text{T}) = 1.21$ at zero-field— comparing well with $\gamma = 1.25$ found for BTZ35 by Kleemann et. al.— and $T_g(6\text{T}) = 40.66\text{K}$ with $\gamma(6\text{T}) = 0.79$ at 6T-field.^[24]

$$\text{MD}_3(\%) = \{\varepsilon'_3(H) \div \varepsilon'_3(0) - 1\} \times 100 \quad (4)$$

It is to be noted that the finite & negative harmonic $\text{MD}_3(\%)$ occurs over roughly the same temperature-window with the positive fundamental MD. Here we can say re-phasing of spatially separated magnetic phases is responsible for the observed harmonic ε'_3 -signal. To further explore the nature of relaxations, non-linear dielectric coefficient (a_3) has been evaluated in respective temperature window.^[25]

$$a_3 = -\varepsilon'_3 \div \varepsilon'^4 \quad (5)$$

Figure 4(c) shows the obtained dielectric non-linearity where, at high temperatures nearly constant a_3 signifies para-electric like region of the system with least correlated dipoles. On decreasing temperature, at $\sim 125\text{K}$ a rise in slope of $a_3(T)$ features relaxor behaviour. On further cooling below 90K a steep increase in a_3 manifests growth of more “glass-like” behaviour in the relaxor. Monotonous increase in temperature dependence of a_3 from para-

electric to relaxor behaviour at $\sim T_N$, further featuring glassy-like behaviour in relaxor below T_{WFM} marks non-linear magneto-dielectricity in the system.

Harmonic signal is H -dependent and exists ($\epsilon'_3(T, H) \neq 0$) only down to the freezing temperature $\sim 50K$ of the segmented dynamics; yielding $MD_3 \neq 0$ over the T -window hosting dynamically-activated dipoles. Over 80-160K, $\epsilon'_3(T)$ -signal decreases under the applied H -field, giving negative MD_3 . Expectedly, under-field de-correlation of dipoles relaxing at low-frequencies (yielding $MD > 0$) also thermally randomizes the 'higher-moments' thereby decreasing the harmonic response.

Conclusions

We have analyzed the signatures of interacting-dipole structures featuring vitreous relaxation kinetics upon cooling below the AFM transition and the emergence of weak ferromagnetic nano-phase at $T_W \sim 110K$, in the AFM matrix ($T_N = 123K$). Alterations of dipoles' correlation-status are allied with the system's magnetic evolution and reflect in the magneto-dielectric signals, upon magnetic field application. In respective temperature regime, spin-lattice coupling has been established in $Ca_3Mn_2O_7$ by analyzing its Raman spectra. Observed second-harmonic magneto-dielectricity is some two orders of magnitude larger, vis-à-vis that obtained in the fundamental response. Structural, magnetic, and electrical coupling in this Ruddlesden-Popper compound is the consequence of its layered structure, which is found to exhibit a topological character. Hence, the ME-coupling can be tailored in its thin-film or nano-fiber formations, where the exclusive features can be enhanced/suppressed by dimensional reduction and intrinsic strain. Furthermore, chemically-doped variants may be investigated to tune the magneto-electric functionality.

Acknowledgments

Suresh Bhardwaj (UGC-DAE CSR) is thankfully acknowledged for his technical help and facilitation of the dielectric-measurements. We extend our sincere thanks to Mr. Ajay Rathore (UGC-DAE CSR) for help with Raman measurements.

References

- [1] B. V. Beznosikov and K. S. Aleksandrov, *Crystallography Reports*, **2000**, 45, 792-798.
- [2] T. Kimura, Y. Tomioka, H. Kuwahara, A. Asamitsu, M. Tamura, and Y. Tokura, *Science*, **1996**, 274, 1698-1701.
- [3] Y. K. Tang, X. Ma, Z. Q. Kou, Y. Sun, N. L. Di, Z. H. Cheng, and Q. A. Li, *Physical Review B*, **2005**, 72, 132403.
- [4] N. A. Benedek and C. J. Fennie, *Physical Review Letters*, **2011**, 106, 107204.
- [5] A. T. Mulder, N. A. Benedek, J. M. Rondinelli, & C. J. Fennie, *Advanced Functional Materials*, **2013**, 23, 4810-4820.
- [6] Y.S. Oh, X. Luo, F.T. Huang, Y. Wang, and S.-W. Cheong, *Nature Materials*, **2015**, 14, 407.
- [7] X.Q. Liu, J.W. Wu, X.X. Shi, H.J. Zhao, H.Y. Zhou, R.H. Qiu, W.Q. Zhang and X.M. Chen, *Applied Physics Letters*, **2015**, 106, 202903.
- [8] A.B. Harris, *Physical Review B*, **2011**, 84, 064116.
- [9] M. Liu, Y. Zhang, L.F. Lin, L. Lin, S. Yang, X. Li. Y. Wang, S. Li, Z. Yan, X. Wang, X.G. Li, S. Dong and J.M. Liu, *Applied Physics Letters*, **2018**, 113, 022902.
- [10] P. Sahlot, G. Sharma, V.G. Sathe, A.K. Sinha, and A.M. Awasthi, *Preprint arXiv:1903.05995*, **2019**.
- [11] P. Sahlot, A. Jana, and A.M. Awasthi, *AIP Conference Proceedings*, **2018**, 1942, 130009.
- [12] P. Sahlot and A.M. Awasthi, *Journal of Magnetism and Magnetic Materials*, **2019**, DOI: 10.1016/j.jmmm.2019.165732.
- [13] M. N. Iliev, S. Jandl, V. N. Popov, A. P. Litvinchuk, J. Cmaidalka, R.L. Meng, & J. Meen, *Physical Review B*, **2005**, 71, 214305.
- [14] J. López-Pérez and J. Íñiguez, *Physical Review B*, **2011**, 84, 075121.

- [15] W. Zhong, and D. Vanderbilt, *Physical Review Letters*, **1995**, 74, 2587.
- [16] N. Sai, and D. Vanderbilt, *Physical Review B*, **2000**, 62, 13942.
- [17] W. Zhu, L. Pi, Y. Huang, S. Tan, and Y. Zhang, *Applied Physics Letters*, **2012**, 101, 192407.
- [18] R. Gerhardt, *Journal of Physics and Chemistry of Solids*, **1994**, 55, 1491-1506.
- [19] R. Pirc, and R. Blinc, *Physical Review B*, **1999**, 60, 13470.
- [20] S. Miga, J. Dec, and W. Kleemann, *In Ferroelectrics- Characterization and Modeling* (Ed. Mickaël Lallart, InTech),. ISBN 978-953-307-455-9, **2011**.
- [21] S. Ikeda, H. Kominami, K. Koyama, and Y. Wada, *Journal of Applied Physics*, **1987**, 62, 3339-3342.
- [22] K. Binder and J.D. Reger, *Advances in Physics*, **1992**, 41, 547-627.
- [23] R. Pirc, B. Tadić, and R. Blinc, *Physica B: Condensed Matter*, **1994**, 193, 109-115.
- [24] W. Kleemann, S. Miga, J. Dec, and J. Zhai, *Applied Physics Letters*, **2013**, 102, 232907.
- [25] V. Bobnar, Z. Kutnjak, R. Pirc, R. Blinc, & A. Levstik, *Physical review letters*, **2000**, 84, 5892.